JACS
JOURNAL OF THE AMERICAN CHEMICAL SOCIETY

COMMUNICATION

pubs.acs.org/JACS

Characterization of Hepatitis B Virus Capsids by Resistive-Pulse Sensing

Kaimeng Zhou,[‡] Lichun Li,[§] Zhenning Tan,[§] Adam Zlotnick,[§] and Stephen C. Jacobson*[,‡]

[‡]Department of Chemistry and [§]Department of Molecular and Cellular Biochemistry, Indiana University, Bloomington, Indiana 47405

Supporting Information

ABSTRACT: We report characterization of hepatitis B virus (HBV) capsids by resistive-pulse sensing through single track-etched conical nanopores formed in poly(ethylene terephthalate) membranes. The pores were ~40 nm in diameter at the tip, and the pore surface was covalently modified with triethylene glycol to reduce surface charge density, minimize adsorption of the virus capsids, and suppress electroosmotic flow in the pore. The HBV capsids were assembled in vitro from Cp149, the assembly domain of HBV capsid protein. Assembled $T = 3$ (90 Cp149 dimer) and $T = 4$ (120 dimer) capsids are 31 and 36 nm in diameter, respectively, and were easily discriminated by monitoring the change in current as capsids passed through an electrically biased pore. The ratio of the number of $T = 3$ to $T = 4$ capsids transiting a pore did not reflect actual concentrations, but favored transport of smaller $T = 3$ capsids. These results combined with longer transit times for the $T = 4$ capsids indicated that the capsids must overcome an entropic barrier to enter a pore.

Nanopores and nanochannels exhibit unique transport properties[1] and have a number of potential applications.[2] Of particular interest is developing label-free, nondestructive techniques for rapid sensing, characterization, and sorting of particles with nanometer dimensions. The resistive-pulse technique[3] measures changes in ion current resulting from transit of particles through an electrically biased nanopore filled with electrolyte. As sensing elements, protein pores,[4] e.g., α-hemolysin, exhibit highly reproducible pore composition and dimensions but lack robustness when suspended in lipid bilayers. Alternatively, micro- and nanofabrication techniques are used to fabricate solid-state and synthetic nanopores[5,6] with a wide range of well-defined geometries and dimensions. Forming these pores parallel or perpendicular to the substrate surface permits straightforward integration with other device features. Solid-state and synthetic nanopores exhibit ion depletion/concentration,[7−9] ion permittivity,[10] enhanced channel conductance,[11] ion current rectification,[12,13] and pressure-induced salt flux rectification.[14,15] The ability to control pore dimensions over a range of length scales permits analysis of a variety of samples, including DNA,[16−18] proteins,[19] viruses,[20] immune complexes,[21] nanoparticles,[22] and small molecules,[23] and similarly designed pores may be used to sequence DNA.[24] In some cases, the molecule of interest, e.g., DNA, must overcome an entropic barrier to enter nanoscale slits[25] and pores.[26] Related to this work is the characterization of viruses with track-etched pores[20] and immune complexes with femtosecond laser-machined pores.[21] In both examples, the studied protein complexes are ~100−150 nm in diameter.

We present a simple method to detect and characterize hepatitis B virus (HBV) capsids with nanopore devices. We used single track-etched conical nanopores formed in poly(ethylene terephthalate) (PET) membranes to discriminate between the 3 MDa $T = 3$ and 4 MDa $T = 4$ HBV capsids. HBV capsid protein can be expressed by *Escherichia coli*, and the capsids can be reassembled in vitro under appropriate conditions, e.g., high ionic strength and protein concentration.[27] $T = 3$ and $T = 4$ icosahedral complexes, composed of 90 and 120 capsid protein dimers, respectively, are formed with a concentration ratio of 1 to 9. Capsid proteins can be reassembled as empty capsids[28] or with nucleic acids.[29] The reassembly process is inherently of interest, and this system offers a unique opportunity to characterize capsid transport, capsid properties, and nanopore properties. The $T = 3$ and $T = 4$ capsids are similar in diameter, 31 and 36 nm, respectively, and have identical surface properties, i.e., chemical composition, charge per unit area, and electrophoretic mobilities. In this work, we used empty capsids formed from Cp149 capsid proteins.

Conical nanopores[30] were fabricated by a two-step etching technique,[31] and the pore surface was covalently modified with triethylene glycol to attenuate the surface charge density, to minimize electrostatic interactions between the capsids and pore wall, and to suppress electroosmotic flow inside the pore (see Supporting Information). To provide an initial estimate of the nanopore dimensions, a scanning electron microscope (SEM) was used to determine the average base diameter, $d_{base} = 590 \pm 140$ nm, from 60 pores in three multipore membranes etched under the same conditions as the single tracked membranes. PET membranes with a single nanopore were mounted in the center of a U-cell. A 10 mM potassium phosphate buffer with 0.1 M KCl (pH 6.8) was placed on both sides of the membrane. A picoammeter-voltage source was used to apply potentials to the U-cell through Ag/AgCl electrodes and monitor the current. After determining the pore resistance, R_{pore}, from a current−voltage (IV) curve, the tip diameter, d_{tip}, was estimated with eq 1:

$$d_{tip} = \frac{4\rho l}{\pi R_{pore} d_{base}} \quad (1)$$

where l is the thickness of the PET membrane (10 μm) and ρ is the specific resistivity of the buffer (71 Ω·cm for 10 mM phosphate buffer with 100 mM KCl). Pores 1, 2, 3, 4, and

Received: September 12, 2010
Published: January 25, 2011

dx.doi.org/10.1021/ja108228x | J. Am. Chem. Soc. 2011, 133, 1618–1621

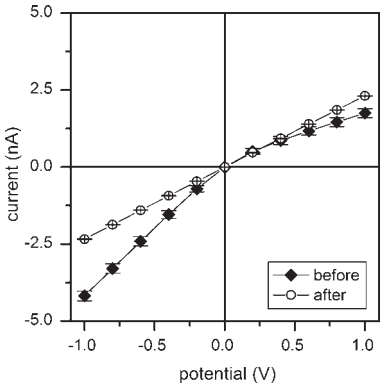

Figure 1. Current−voltage (*IV*) curves of a conical nanopore before and after surface modification with triethylene glycol. The buffer was 10 mM potassium phosphate buffer with 100 mM KCl, and the *IV* data are for pore 1. Error bars are ± σ.

5 had estimated tip diameters of 36 ± 11, 55 ± 13, 53 ± 13, 48 ± 12, and 52 ± 12 nm, respectively. The standard deviations for the tip diameters were determined from the base diameter and resistance measurements. Current measurements provided an approximation of the tip diameters, but a pore with a wider base and narrower tip cannot be readily distinguished from a pore with a narrower base and a wider tip. As we show, the relative transport of $T = 3$ and $T = 4$ capsids through the pore provided a more accurate assessment of the tip diameter.

Membranes with pores 1, 2, and 3 were covalently modified with triethylene glycol for 4 h (see Supporting Information). After modification, the pores did not rectify ion current, i.e., had rectification ratios of 1.0. (The rectification ratio is the absolute value of the ratio of currents measured at potentials of equal magnitude but opposite sign.) Figure 1 shows the *IV* curves for pore 1 before and after modification. For the reaction time of 4 h, 22 of 25 pores were successfully modified and showed *IV* behavior similar to that of pore 1 in Figure 1. The membranes with pores 4 and 5 were covalently modified for a reaction time of only 2 h. As a result, pores 4 and 5 continued to rectify ion current after surface modification, and the rectification ratios were 1.34 and 1.33, respectively.

Next, we demonstrated that the electrically biased pores were capable of distinguishing the two sizes of HBV capsids ($T = 3$ and $T = 4$). A 50 mM HEPES buffer with 1 M NaCl (pH 7.2) and HBV capsids was placed in the half of the U-cell in contact with the nanopore tip, and the virus capsids were translocated through the nanopore electrophoretically. A multifunction data acquisition board controlled through LabVIEW supplied the applied potential and recorded the amplified current signal from the translocation events at 1 or 10 kHz. Figure 2a shows a current trace of 0.5 nM unpurified, reassembled HBV capsids (~10% $T = 3$ capsids and ~90% $T = 4$ capsids). The baseline current was subtracted from the data, and the pulse amplitude (Δi) is the difference between the baseline current and the pulse minimum. In Figure 2a, the small pulses are labeled $T = 3$ capsids and the large pulses $T = 4$ capsids. Figure 2b shows a histogram of Δi obtained from pores 2 and 4. The histograms for both pores are overlaid for comparison, and both data sets showed the presence of two well-resolved distributions. Pore 2 produced maxima in the Δi distributions spread farther apart than the Δi distribution maxima for pore 4. With pore 2, the $T = 3$ and $T = 4$ distributions were confirmed by obtaining histograms of sucrose gradient-purified[32] $T = 3$ and $T = 4$ samples (see Figure 3).

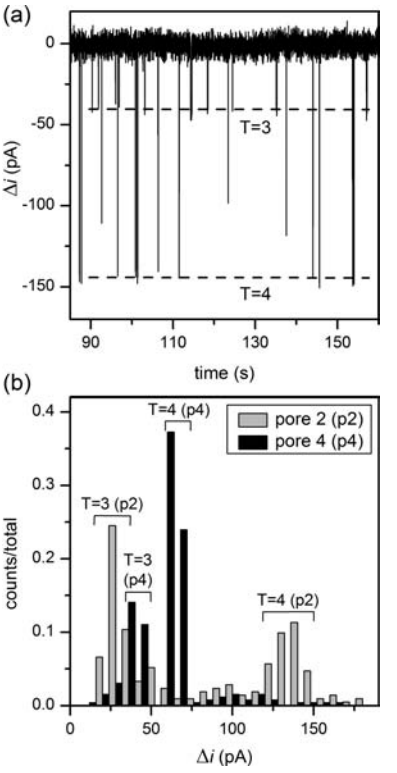

Figure 2. (a) Variation of pulse amplitude (Δi) with time for a mixture of $T = 3$ and $T = 4$ HBV capsids analyzed with pore 2. Dashed lines indicate the current pulses for $T = 3$ and $T = 4$ capsids. The applied potential was 0.3 V. (b) Histogram of Δi for mixtures of $T = 3$ and $T = 4$ HBV capsids characterized with pores 2 and 4. For pore 2, total counts are 212, and $n_3/n_4 = 1.31$. For pore 4, total counts are 263, and $n_3/n_4 = 0.48$. The applied potential was 1 V for pore 4.

Interestingly, the counts from the two distributions in the histogram of the mixture do not reflect the actual concentrations of $T = 3$ and $T = 4$ capsids. In Figure 2b, the ratio of the number of $T = 3$ capsids to $T = 4$ capsids (n_3/n_4) is 1.31 for pore 2 and 0.48 for pore 4, whereas the expected n_3/n_4 is 0.11 for a sample with 10% $T = 3$ capsids and 90% $T = 4$ capsids. These higher than expected ratios suggested that the diameter of the pore tip influenced the transport of $T = 3$ and $T = 4$ capsids differently. Moreover, as a capsid enters a confined space, e.g., a nanopore, entropy is lost. A greater entropic barrier for $T = 4$ capsids is expected than for the $T = 3$ capsids due to their size difference, and this entropic barrier becomes more significant as the capsid diameter approaches the tip diameter of the pore. Equation 2 describes the partition coefficient for spherical particles entering a circular pore:

$$K_T = \left(1 - \frac{d_{cap,T}}{d_{tip}}\right)^2 \quad (2)$$

where K_T is the partition coefficient for $T = 3$ or 4 and d_{cap} is the capsid diameter (31 nm for $T = 3$ capsids and 36 nm for $T = 4$ capsids). Therefore, we can determine n_3/n_4 in terms of pore diameter with eq 3,

$$\frac{n_3}{n_4} = \frac{C_3 K_3}{C_4 K_4} \quad (3)$$

where C_3/C_4 is the relative concentration of the capsids. Figure 4 shows that a rapid increase in n_3/n_4 is expected as the diameter of the

dx.doi.org/10.1021/ja108228x | J. Am. Chem. Soc. 2011, 133, 1618–1621

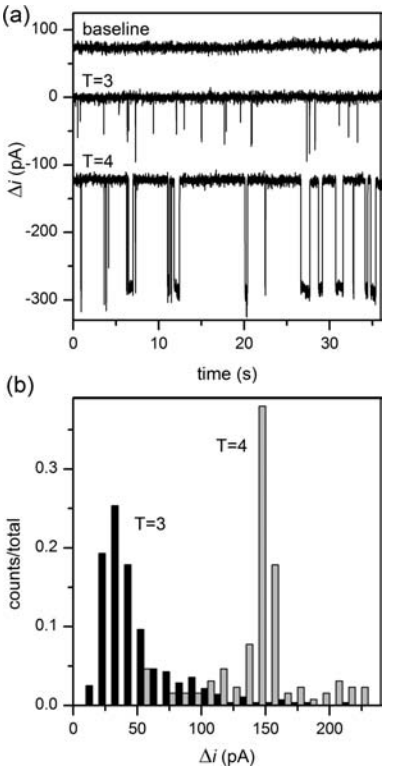

Figure 3. (a) Variation of Δi with time for no capsids (baseline), purified $T = 3$ capsids, and purified $T = 4$ capsids analyzed with pore 2. The applied potential was 0.5 V. (b) Histogram of Δi for purified $T = 3$ and $T = 4$ capsids characterized with pore 2. $n_3 = 200$, and $n_4 = 250$.

pore tip decreases toward the $T = 4$ capsid diameter (36 nm). For pores 1, 2, 3, and 4, n_3/n_4 is 1.37, 1.31, 0.88, and 0.48, respectively. Substituting these n_3/n_4 ratios and $C_3/C_4 = 0.11$ into eq 3 gives estimated pore diameters of 38, 38, 39, and 41 nm for pores 1, 2, 3, and 4, respectively. These pore diameters are underestimated because the capsid diameters were from crystallographic measurements of capsids that do not include a hydration layer. Figure 4 shows how sensitive n_3/n_4 is to the pore diameter when the pore diameter is similar to the capsid diameter. The average tip diameter estimated from the data in Figure 4 is 40.5 ± 1.5 nm. Error for the tip diameter is considerably smaller than the errors estimated by eq 1, which are inferred from the base diameters and their associated errors. The results also indicated the pore tips have nearly circular cross sections that permit passage of the spherical capsids.

Further, we analyzed the transit times (Δt) of the $T = 3$ and $T = 4$ capsids. In Figure 5, histograms of Δt for the $T = 3$ and $T = 4$ capsids exhibited an exponential decay and were fitted with a single exponential. The fits showed that the time constant (τ) for the $T = 4$ capsids was 30.8 ± 0.4 ms, and τ for the $T = 3$ capsids was 6.3 ± 0.5 ms. The difference in τ is consistent with a higher entropic barrier for $T = 4$ capsids to enter the pore.

With purified $T = 4$ capsids, we investigated how the applied potential (V_{app}) influenced Δi and Δt. From histograms of Δi at different applied potentials, Figure 6a shows that the pulse amplitudes scaled linearly with applied potential, and $1/\tau$ varied nonlinearly with applied potential. A decrease in τ with increasing applied potential was anticipated because the applied potential helped capsids overcome the barrier to enter the pore. However, additional physical processes, such as structural distortions of the capsid or adsorption of the capsid to the pore wall may add to Δt,

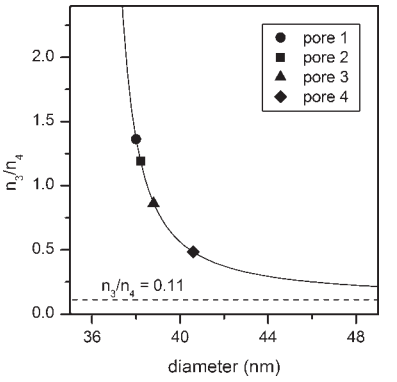

Figure 4. Variation of n_3/n_4 with pore diameter for pores 1, 2, 3, and 4. The solid line is calculated with eq 3, and the dashed line is $n_3/n_4 = 0.11$.

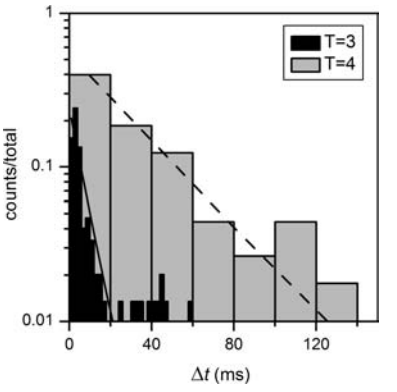

Figure 5. Histogram of transit time (Δt) for $T = 3$ and $T = 4$ capsids. The data are from pore 2 in Figure 2. The solid and dashed lines are exponential fits to transit times for $T = 3$ and $T = 4$ capsids, respectively.

especially at lower applied potentials. Electrostatic interactions are suppressed by covalent modification of the pore surface and the high ionic strength buffer.

Small variations in the tip diameter, nanopore shape, and surface roughness from the fabrication process led to each nanopore having a different working potential range. For example, pore 1 required an applied potential of 7 V to produce pulses with a good signal-to-noise ratio, whereas pores 2 and 3 required 0.3 and 0.2 V, respectively, to obtain similar results. This observation is consistent with the change in the ion conductance ($\Delta G = \Delta i/V_{app}$) as capsids passed through the pores. The average pulse amplitude (Δi) was calculated from data similar to Figure 2a for $T = 4$ capsids and divided by the applied potential (V_{app}). ΔG was 560 pS for pore 1, 470 pS for pore 2, and 650 pS for pore 3. Despite markedly different applied potentials, ΔG was similar for pores 1, 2, and 3. If the pores were circularly symmetric, smaller pores should exhibit a larger ΔG as a capsid passed through the pore. Pore 3 had a slightly higher ΔG than pores 1 and 2, which indicated that capsids fit more snugly in pore 3 and, subsequently, displaced a larger fraction of electrolyte during the measurement.

Variation of $\Delta i_4/\Delta i_3$ with τ_4/τ_3 in Figure 6b shows a linear relationship for pores 1, 2, and 3, which are operated with different applied potentials, but have similar surface chemistries, e.g., covalent modification of the pore surface with triethylene glycol. This finding permits direct comparison between data from different pores. As mentioned above, the ion current did not rectify on pores 1, 2, and 3 after surface modification. Pore 4

dx.doi.org/10.1021/ja108228x | J. Am. Chem. Soc. 2011, 133, 1618–1621

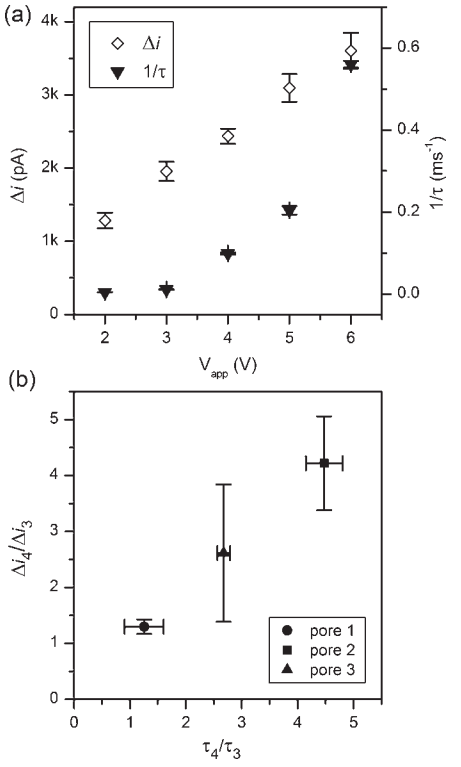

Figure 6. (a) Variation of Δi and $1/\tau$ with applied potential (V_{app}) for $T = 4$ capsids analyzed with pore 5. (b) Variation of $\Delta i_4/\Delta i_3$ with τ_4/τ_3 for pores 1, 2, and 3. Error bars are $\pm \sigma$.

rectified current after surface treatment, and the τ_4/τ_3 ratio was larger than predicted. The presence of electroosmotic flow, which opposed the direction of electrophoretic transport of the capsids, increased the transit time of the capsids, and thus, increased τ_4 to a greater extent than τ_3.

In conclusion, current pulses from $T = 3$ and $T = 4$ capsids were easily resolved on electrically biased pores with tip diameters of ~40 nm. To obtain a histogram of Δi with a representative concentration distribution would require much larger pores with >100 nm, at the cost of a lower signal-to-noise ratio and a smaller difference in Δi between particle sizes. In addition, suppressing electroosmotic flow was necessary for capsids to enter pores electrophoretically. However, the minimal electroosmotic flow in pores 4 and 5 slowed particle transport through the pore, increasing Δt and subsequently improving measurement precision.

■ ASSOCIATED CONTENT

Ⓢ Supporting Information. Nanopore fabrication, covalent surface modification, and complete ref 24. This material is available free of charge via the Internet at http://pubs.acs.org.

■ AUTHOR INFORMATION

Corresponding Author
jacobson@indiana.edu

■ ACKNOWLEDGMENT

This work was supported in part by NSF CHE-0750295 and NSF CHE-0832651 for K.Z. and S.C.J. and by NIH R01 AI077688 for L.L., Z.T., and A.Z. We thank Prof. Bogdan Dragnea for insightful discussions.

■ REFERENCES

(1) Schoch, R. B.; Han, J.; Renaud, P. *Rev. Mod. Phys.* **2008**, *80*, 839–883.
(2) Kovarik, M. L.; Jacobson, S. C. *Anal. Chem.* **2009**, *81*, 7133–7140.
(3) DeBlois, R. W.; Bean, C. P. *Rev. Sci. Instrum.* **1970**, *41*, 909–916.
(4) Bayley, H.; Cremer, P. S. *Nature* **2001**, *413*, 226–230.
(5) Dekker, C. *Nat. Nanotechnol.* **2007**, *2*, 209–215.
(6) Martin, C. R.; Siwy, Z. S. *Science* **2007**, *317*, 331–332.
(7) Pu, Q.; Yun, J.; Temkin, H.; Liu, S. *Nano Lett.* **2004**, *4*, 1099–1103.
(8) Wang, Y.-C.; Stevens, A. L.; Han, J. *Anal. Chem.* **2005**, *77*, 4293–4299.
(9) Zhou, K.; Kovarik, M. L.; Jacobson, S. C. *J. Am. Chem. Soc.* **2008**, *130*, 8614–8616.
(10) Siwy, Z.; Kosinska, I. D.; Fulinski, A.; Martin, C. R. *Phys. Rev. Lett.* **2005**, *94*, 048102.
(11) Stein, D.; Kruithof, M.; Dekker, C. *Phys. Rev. Lett.* **2004**, *93*, 035901.
(12) Siwy, Z. S. *Adv. Funct. Mater.* **2006**, *16*, 735–746.
(13) Kovarik, M. L.; Zhou, K.; Jacobson, S. C. *J. Phys. Chem. B* **2009**, *113*, 15960–15966.
(14) Szymczyk, A.; Zhu, H. C.; Balannec, B. *J. Phys. Chem. B* **2010**, *114*, 10143–10150.
(15) Goldsmith, J.; Martens, C. C. J. *Phys. Chem. Lett.* **2010**, *1*, 528–535.
(16) Li, J.; Gershow, M.; Stein, D.; Brandin, E.; Golovchenko, J. A. *Nat. Mater.* **2003**, *2*, 611–615.
(17) Chen, P.; Gu, J. J.; Brandin, E.; Kim, Y. R.; Wang, Q.; Branton, D. *Nano Lett.* **2004**, *4*, 2293–2298.
(18) Storm, A. J.; Storm, C.; Chen, J. H.; Zandbergen, H.; Joanny, J. F.; Dekker, C. *Nano Lett.* **2005**, *5*, 1193–1197.
(19) Sexton, L. T.; Horne, L. P.; Sherrill, S. A.; Bishop, G. W.; Baker, L. A.; Martin, C. R. *J. Am. Chem. Soc.* **2007**, *129*, 13144–13152.
(20) DeBlois, R. W.; Wesley, R. K. A. *J. Virol.* **1977**, *23*, 227–233.
(21) Uram, J. D.; Ke, K.; Hunt, A. J.; Mayer, M. *Angew. Chem., Int. Ed.* **2006**, *45*, 2281–2285.
(22) Lee, S.; Zhang, Y. H.; White, H. S.; Harrell, C. C.; Martin, C. R. *Anal. Chem.* **2004**, *76*, 6108–6115.
(23) Heins, E. A.; Siwy, Z. S.; Baker, L. A.; Martin, C. R. *Nano Lett.* **2005**, *5*, 1824–1829.
(24) Branton, D.; et al. *Nat. Biotechnol.* **2008**, *26*, 1146–1153.
(25) Han, J.; Turner, S. W.; Craighead, H. G. *Phys. Rev. Lett.* **1999**, *83*, 1688–1691.
(26) Kowalczyk, S. W.; Tuijtel, M. W.; Donkers, S. P.; Dekker, C. *Nano Lett.* **2010**, *10*, 1414–1420.
(27) Katen, S.; Zlotnick, A. *Methods in Enzymology: Biothermodynamics*; Elsevier Academic Press Inc: San Diego, 2009; Vol. 455, Part A, pp 395−417.
(28) Zlotnick, A.; Cheng, N.; Conway, J. F.; Booy, F. P.; Steven, A. C.; Stahl, S. J.; Wingfield, P. T. *Biochemistry* **1996**, *35*, 7412–7421.
(29) Porterfield, J. Z.; Dhason, M. S.; Loeb, D. D.; Nassal, M.; Stray, S. J.; Zlotnick, A. *J. Virol.* **2010**, *84*, 7174-7184.
(30) Apel, P. Y.; Korchev, Y. E.; Siwy, Z.; Spohr, R.; Yoshida, M. *Nucl. Instrum. Methods Phys. Res., Sect. B* **2001**, *184*, 337–346.
(31) Wharton, J. E.; Jin, P.; Sexton, L. T.; Horne, L. P.; Sherrill, S. A.; Mino, W. K.; Martin, C. R. *Small* **2007**, *3*, 1424–1430.
(32) Zlotnick, A.; Palmer, I.; Kaufman, J. D.; Stahl, S. J.; Steven, A. C.; Wingfield, P. T. *Acta Crystallogr., Sect. D* **1999**, *55*, 717–720.